

Coarse-grained modeling of thermochemical nonequilibrium using the multigroup maximum entropy quadratic formulation

Maitreyee P. Sharma *Department of Aerospace Engineering, University of Illinois at Urbana-Champaign, Urbana, Illinois 61801, USA*

Yen Liu

NASA Ames Research Center, Moffett Field, California 94035, USA

Marco Panesi*

Department of Aerospace Engineering, University of Illinois at Urbana-Champaign, Urbana, Illinois 61801, USA

(Received 9 July 2019; published 16 January 2020)

This work addresses the construction of a reduced-order model based on a multigroup maximum entropy formulation for application to high-enthalpy nonequilibrium flows. The method seeks a piecewise quadratic representation of the internal energy-state populations by lumping internal energy levels into groups and by applying the maximum entropy principle in conjunction with the method of moments. The use of higher-order polynomials allows for an accurate representation of the logarithm of the distribution of the low-lying energy states, while preserving an accurate description of the linear portions of the logarithm of the distribution function that characterize the intermediate- and high-energy states. A comparison of the quadratic and the linear reconstructions clearly demonstrates how the higher-order reconstruction provides a more accurate representation of the internal population distribution function at a modest increase in the computational cost. Numerical simulations carried out under conditions relevant to hypersonic flight reveal that the proposed model is able to capture the dynamics of the nonequilibrium distribution function using as few as three groups, thereby reducing the computational costs for simulations of nonequilibrium flows.

DOI: [10.1103/PhysRevE.101.013307](https://doi.org/10.1103/PhysRevE.101.013307)

I. INTRODUCTION

Over the past decade there has been renewed interest in high-fidelity modeling of nonequilibrium hypersonic flows. With the increasing availability of computational resources it is now possible to compute state-specific kinetic data by leveraging *ab initio* potential energy surfaces and quasiclassical trajectory calculations [1–11]. Although state-to-state (StS) simulations [12–14] yield the most accurate description of the nonequilibrium population distribution, they are prohibitively expensive and cannot be used in computational fluid dynamics calculations [15–19]. To overcome the limitations of the StS methodology, various researchers have developed reduced-order models. The simplest method of reduction is the multitemperature model [20–24], where macroscopic rate coefficients and relaxation energy parameters are expressed in terms of one or more temperatures. The need for an accurate description of nonequilibrium phenomena (e.g., the dynamics of the internal distribution function) has led to the construction of a new class of models, where the internal population distribution is described using functions that have local instead of global support over the internal energy space. To this aim, the energy states are lumped together into groups and their population is prescribed in terms of a predetermined distribu-

tion (e.g., uniform, Boltzmann, etc.). Gordiets *et al.* [25] first proposed the use of multiple distributions patched together to represent the vibrational population during a nonequilibrium chemical relaxation. In this work, the energy levels were grouped based on their relaxation mechanisms, with the lower-energy levels having a Treanor [26]–like distribution, while the intermediate and the high-lying levels followed Boltzmann distributions at different temperatures. Kustova *et al.* [24] extended the model to include transport properties using kinetic theory. The computed transport properties were then used to simulate nozzle expansion flows [27,28] and the population distribution function showed a good agreement with the StS results. More recently, a number of papers on the complexity reduction for state-specific chemical kinetics have been published [16,29–39]. The approach followed is very similar in all cases; a piecewise distribution is used to reconstruct the population of the internal levels. The main differences are related to the assumption regarding the specification of the group distribution and temperatures; while some models assume fast equilibration of the group temperature with the kinetic temperature, others determine the evolution of the temperature within each group, by solving additional equations.

This work addresses the extension of the multigroup maximum entropy method (MGME) [30–32,38] to allow for reconstruction of the population distribution using high-order polynomials. Traditionally, maximum-entropy-based methods [40–43] have been used as a “scaling law” to generate large

*mpanesi@illinois.edu

matrices of state-specific cross sections [42], leveraging the maximum entropy functional form. For example, Kulakhmetov *et al.* [43] used maximum entropy theory to derive analytical expressions for the state-specific cross sections. The authors referred to this method as ME-QCT. Here, instead, the multigroup maximum entropy method is used to derive a reduced-order model. Following the work of Liu *et al.* [30–32] the maximum entropy principle subject to a series of constraints (i.e., mass, energy, etc.) is used to reconstruct the population of the energy states within each group. A similar approach was used to derive conservation equations for polydisperse multiphase flows [44]. The multigroup maximum entropy linear model was first published in 2010 [30]; there the macroscopic mass and internal energy equations for energy groups were obtained in a coupled manner from the zeroth-order and first-order moments of the master equations. The formulation was later extended to higher orders [31] and to general collisional and radiative processes [32,39]. Finally, Munafò *et al.* [38] modified the formulation to introduce multiple temperatures per group. In its original formulation, the MGME method requires knowledge of the state-specific rate coefficients, which for more complicated systems can be prohibitively expensive. To overcome this problem, recently Macdonald *et al.* [45,46] applied the MGME methodology to quasiclassical trajectory calculations for direct determination of the grouped reaction rate parameters.

Under strong nonequilibrium conditions, the linear multigroup maximum entropy method [32] requires a large number of groups to accurately capture the dynamics of the distribution function. To overcome the limitations of the previous models, the present work focuses on the implementation of a robust and computationally efficient method using the multigroup maximum entropy quadratic formulation. The introduction of a high-order reconstruction in the multigroup maximum entropy modeling technique allows one to capture curvature in the population distribution function (i.e., low-lying energy states) with a reduced number of groups, thus addressing the limitations of the linear reconstruction model.

The paper is arranged as follows: Sec. II describes the state-specific chemical kinetics of the $N_2(^1\Sigma_g^+)$ - $N(^4S_u)$ system, which includes inelastic collisions and chemical reactions of the rovibrational energy states. The details of the master equations are also discussed. Section III presents the formulation of the multigroup maximum entropy quadratic model. The results of the numerical simulations and model validation are presented in Sec. IV. Finally, concluding remarks on this work are given in Sec. V.

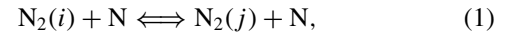
II. CHEMICAL SYSTEM

A. State-to-state kinetics

The multigroup quadratic model developed is applicable for any system at thermo-chemical nonequilibrium. To illustrate the methodology, we choose as an example a pure nitrogen gas mixture, $N_2(^1\Sigma_g^+)$ - $N(^4S_u)$, system. In this system, rovibrational energy transfer (excitation-deexcitation processes) and chemical reactions (dissociation-recombination processes) between the molecules and the atoms are considered.

The $N_2(^1\Sigma_g^+)$ molecule has 9390 rovibrational levels. The first 7421 levels are bound levels and the remaining are predissociated or quasibound. Here, we limit our analysis to the bound energy levels of the molecules, given that the quasibound levels are best characterized by linear or even constant reconstruction [35,36]. The StS kinetics data for this system are obtained from *ab initio* calculations performed at NASA Ames Research Center [1–4,12]. The rovibrational levels are sorted in increasing order of their energy, with no distinction between the rotation and the vibration levels. When every internal energy state is treated individually no decoupling of the rotation and vibration energy states is needed.

The StS chemical kinetics of the $N_2(^1\Sigma_g^+)$ - $N(^4S_u)$ system can be written as



The indices i and j in the reaction represent the rovibrational level of the $N_2(^1\Sigma_g^+)$ molecule. Reaction (1) includes inelastic and exchange reactions [16]. The other pair of reactions, (2), is the dissociation-recombination reactions. For some of the excitation processes the probability of occurrence is so low that they are not observed in the quasiclassical trajectory calculations and hence are ignored. These reactions, (1) and (2), lead to more than 44×10^6 possible rovibrational dissociation and energy transfer interactions that comprise the chemical kinetics of the $N_2(^1\Sigma_g^+)$ - $N(^4S_u)$ system.

B. Microscopic governing equations

Let n_i , g_i , and ε_i denote the population, degeneracy, and energy of rovibrational level i of the N_2 molecule, n_N the population of N atoms, and I_n the set of bound energy levels. The microscopic master equation governing the population density of N_2 molecules for reactions (1) and (2) can be written as

$$\frac{dn_i}{dt} = \sum_{j \in I_n} [-k_{i,j} n_i n_N + k_{j,i} n_j n_N] + [-k_i^d n_i n_N + k_i^r n_N^2 n_N], \quad i \in I_n. \quad (3)$$

The concentration of the chemical species is a function of time alone, i.e., the mixture is assumed to be spatially homogeneous, and the simulations are ordinary differential equations in time. The first two terms in the master equation denote the excitation and deexcitation processes. The last two terms denote the change in the individual state population density due to dissociation and recombination processes.

The excitation rate coefficients from level i to level j are denoted $k_{i,j}$ and the dissociation rate coefficients are denoted k_i^d . These rate coefficients are calculated using an Arrhenius fit where the fit parameters are obtained from calculations done at NASA Ames Research Center. The deexcitation rate coefficients $k_{j,i}$ and recombination rate coefficients k_i^r are

computed using the relations of detailed balance,

$$k_{j,i} = k_{i,j} \frac{g_i}{g_j} \exp \left[\frac{-(\varepsilon_i - \varepsilon_j)}{k_B T} \right], \quad (4)$$

$$k_i^r = k_i^d \frac{g_i Q_{N_2}^r}{(g_N Q_N^r)^2} \exp \left[\frac{-(\varepsilon_i - 2\varepsilon_N)}{k_B T} \right], \quad (5)$$

where

$$Q_N^r = \left(\frac{2\pi m_N k_B T}{h^2} \right)^{\frac{3}{2}}, \quad Q_{N_2}^r = \left(\frac{2\pi m_{N_2} k_B T}{h^2} \right)^{\frac{3}{2}}. \quad (6)$$

The symbol k_B represents the Boltzmann constant and h is the Planck constant. Q^r is the translation partition function, with m being the mass of a single atom or molecule per unit volume. The translational temperature of the gas is denoted T .

The microscopic master equation discussed in this section is the pivotal point in the development of the quadratic model characterizing chemical nonequilibrium. The model order-reduction technique adopted in this paper is discussed in the following section.

III. MODEL FRAMEWORK

The maximum entropy formulation implies that the logarithm of the distribution function can be represented by a polynomial of the internal energy. Using multiple groups indicates that the representation is piecewise. The formulation of the multigroup maximum entropy method, using a linear reconstruction, was presented by Liu *et al.* [30], and later it was extended to higher orders using an arbitrary-degree polynomial representation [31,32]. Although the formulation was expressed in a general form, only a linear representation was actually implemented. In this section we present the quadratic representation, for the purpose of clarity and completeness.

A. Method of moments and maximum entropy principle

In statistics, the method of moments is a tool used to estimate population distributions of random variables based on the law of large numbers. Here, this powerful technique is applied to obtain governing equations that describe the internal energy-space population distribution in thermal and chemical nonequilibrium flows.

The energy value, X , is a discrete random variable whose possible realizations are ε_i , the energy of the internal states of the molecule, and $P\{X = \varepsilon_i\}$ is the probability that a molecule chosen at random will belong to the i th state. When the system is at equilibrium, $P\{X = \varepsilon_i\}$ is given by the Boltzmann distribution,

$$P\{X = \varepsilon_i\} = \frac{n_i}{n_{\text{tot}}} = \frac{g_i \exp \left[-\frac{\varepsilon_i}{k_B T} \right]}{\sum_{j \in I_n} g_j \exp \left[-\frac{\varepsilon_j}{k_B T} \right]}, \quad (7)$$

where n_i and g_i are the population and degeneracy of energy state i , and $n_{\text{tot}} = \sum_{i \in I_n} n_i$ is the total number of molecules. Since it is impractical to solve the microscopic master equation [Eq. (3)], and in some cases the problem becomes intractable, the method of moments is adopted to describe thermal and chemical nonequilibrium processes. The number of molecules in a macroscopic quantity of the gas is extremely large, of the order of Avogadro's number, therefore, the law

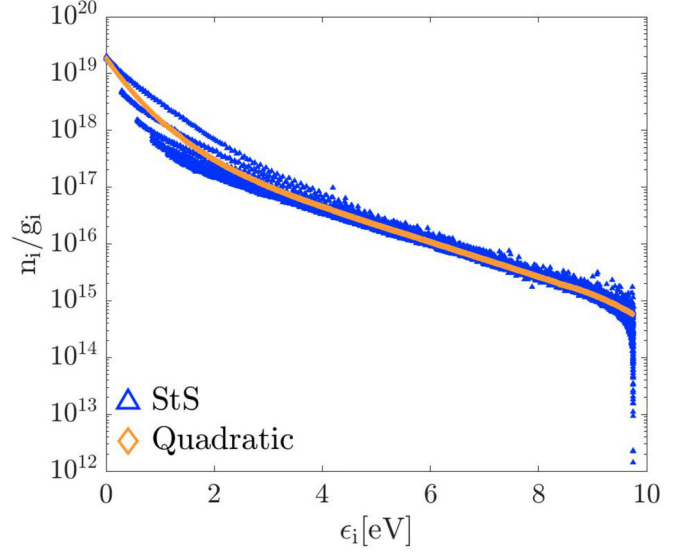


FIG. 1. Nonequilibrium state-to-state population distribution function (blue triangles) and a seven-group quadratic piecewise reconstruction (orange diamonds).

of large numbers can be applied to estimate the population distribution function in energy space. The probability mass function (PMF) is taken to be a quadratic function to obtain a good reconstruction of the trends observed in typical nonequilibrium StS population distribution functions (Fig. 1).

The form of the estimated PMF derived in this paper is based on the maximum entropy principle, which enforces the population distribution function of a system to be such that the entropy of the system is maximized while satisfying some constraints. This results in an (over-)constrained problem (see [32,47] for a detailed derivation) for the most probable macrostate of the system which maximizes entropy. To solve this constrained maximization problem, the method of Lagrange multipliers is employed in order to satisfy the constraints.

B. Constraints on the distribution function

Since the population of the internal levels cannot be described accurately by a single second-order polynomial, the state space is divided into groups of equal energy intervals, each characterized by an independent distribution. The logarithm of the distribution is then approximated using a piecewise quadratic polynomial. Characterization of the quadratic function requires three parameters, which can be determined by taking moments of the energy. The moments used in this work are:

i. The zeroth-order moment, $\sum_{i \in I_g} n_i = n_g$, corresponds to the mass constraint within each group.

ii. The first-order moment, $\sum_{i \in I_g} n_i \varepsilon_i = e_g$, implies the conservation of energy within each group.

iii. The second-order moment, $\sum_{i \in I_g} n_i \varepsilon_i^2 = f_g$, denotes the square of the energy within each group. This constraint is required due to the choice of a quadratic reconstruction function for the PMF.

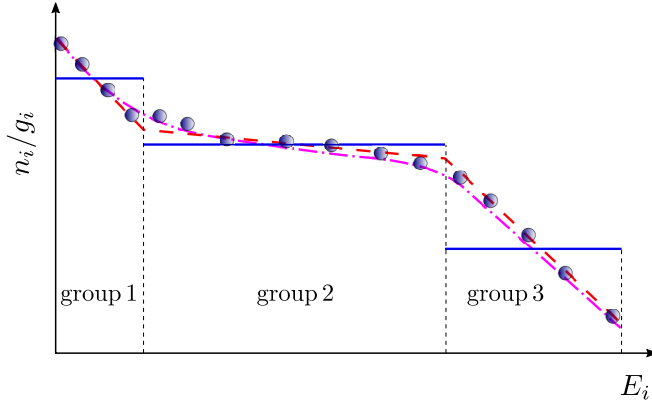


FIG. 2. Different types of reconstruction functions estimating the actual distribution function in each group; constant (solid blue line), linear (dashed red line), and quadratic (dotted-dashed pink line); symbols denote the actual distribution function.

While the first two constraints are related to conservation laws of nature, namely, conservation of mass and conservation of energy, the third constraint is necessary to allow for the higher-order reconstruction, and it does not have any immediate physical meaning. Furthermore, the group model parameters which characterize the PMF are functions of the group moments, $\alpha_g = \alpha_g(n_g, e_g, f_g)$, $\beta_g = \beta_g(n_g, e_g, f_g)$, and $\gamma_g = \gamma_g(n_g, e_g, f_g)$, and they enter the formulation of the quadratic model as Lagrange multipliers. As a result of applying the maximum entropy principle and using these Lagrange multipliers, the form of the PMF for the most probable macrostate which maximizes the entropy of the system is as follows [31,32]:

$$\ln \frac{g_i}{n_i} = \alpha_g + \beta_g \varepsilon_i + \gamma_g \varepsilon_i^2, \quad i \in I_g, \quad (8)$$

$$I_g = \{i \mid \varepsilon_{g-1} < \varepsilon_i \leq \varepsilon_g\}, \quad g = 1, 2, \dots \quad (9)$$

The subscript g denotes the group index and the finite discrete set I_g is given by Eq. (9). The energy of the highest-lying state in the group is represented as ε_g . As discussed in the following subsection, the evolution of these moments in time is solved for in order to obtain the time dependence of the quadratic model parameters. Having obtained the model parameters as a function of time, the transient nonequilibrium population distribution can be reconstructed.

Before moving on to discuss the master equation for the multigroup maximum entropy quadratic model, we take a look at the quadratic model parameters. Figure 2 is a representation of the form of the PMF shown for different approximations of the distribution function with a three-group maximum entropy model. The blue circles are a cartoon representation of the actual distribution in the energy states. The horizontal blue line corresponds to the type of reconstructed population obtained when using only the constant term, α_g , in (8). Increasing the order of the approximation up to the linear term, we obtain a representation as shown by the red lines. Finally, in the quadratic representation, we introduce the quadratic parameter, γ , and the estimated PMF is represented by the pink quadratic curves.

The constant term (blue line in Fig. 2) in the quadratic representation of the energy-state population distribution, α_g , comes from the first constraint, i.e., mass conservation within each group. It can be shown to be related to the number of moles in the group and the zeroth partition function [Eq. (11) for $m = 0$] by the following relations:

$$n_g = \sum_{i \in I_g} n_i,$$

$$n_g = \sum_{i \in I_g} g_i \exp[-\alpha_g - \beta_g \varepsilon_i - \gamma_g \varepsilon_i^2],$$

$$\exp[-\alpha_g] = \frac{n_g}{Q_g}; \quad (10)$$

$${}^m Q_g = \sum_{i \in I_g} g_i \varepsilon_i^m \exp[-\beta_g \varepsilon_i - \gamma_g \varepsilon_i^2]. \quad (11)$$

The linear (β_g) and quadratic (γ_g) parameters are related to the slope and curvature of the logarithm of the PMF by the following relations:

$$\text{slope} = -\beta_g - \gamma_g \varepsilon_i,$$

$$\text{curvature} = \frac{\gamma_g}{(1 + (-\beta_g - \gamma_g \varepsilon_i)^2)^{1.5}}. \quad (12)$$

Since α_g can be written in terms of the other two model parameters, we are only required to solve for β_g and γ_g . Recalling that β_g and γ_g are functions of the group moments, the two conservation constraints on the energy and energy-squared terms are used to obtain the values of these model parameters. These constraints together form a system of coupled nonlinear equations in β_g and γ_g , Eq. (13), which are solved simultaneously to obtain the linear and quadratic parameters. In this work we use an iterative inexact Newton algorithm from the KINSOL Library of the SUNDIALS package [48]:

$$e_g = e_g(\beta_g, \gamma_g) = \sum_{i \in I_g} g_i \varepsilon_i \exp[-\beta_g \varepsilon_i - \gamma_g \varepsilon_i^2],$$

$$f_g = f_g(\beta_g, \gamma_g) = \sum_{i \in I_g} g_i \varepsilon_i^2 \exp[-\beta_g \varepsilon_i - \gamma_g \varepsilon_i^2]. \quad (13)$$

In Eq. (13), the left-hand side is obtained by evolving the moments in time as detailed in the following subsection.

C. Time-varying nonequilibrium distributions

The method of moments along with the maximum entropy principle described above is used to characterize the transient nonequilibrium internal energy population distribution. In order to arrive at the macroscopic moment governing equations, moments of the microscopic master equation, Eq. (3), are taken [31,32]:

$$\begin{aligned} \sum_{i \in I_g} \frac{d(n_i \varepsilon_i^m)}{dt} &= \sum_{i \in I_g} \sum_{h \in \mathbf{N}} \sum_{j \in I_h} [-k_{i,j} \varepsilon_i^m n_i n_N + k_{j,i} \varepsilon_i^m n_j n_N] \\ &+ \sum_{i \in I_g} [-k_i^d \varepsilon_i^m n_i n_N + k_i^r \varepsilon_i^m n_N^2 n_N]. \end{aligned} \quad (14)$$

Here, \mathbf{N} denotes the number of permissible group indices such that union of all the groups spans the whole energy-state

space of the molecule. The collision partner is chosen to be atomic nitrogen and is assumed to be inert. The grouping strategy reduces the number of ordinary differential equations to be solved from the order of the number of rovibrational levels in the molecule to the order of the number of groups chosen to represent the energy space of the molecule. Further, the group rate coefficients are computed and Eq. (14) is rewritten using grouped macroscopic rate coefficients. $K_{g,h}$ denotes the group excitation rate coefficient for the excitation process occurring from group g to group h , and C_g^d represents the group dissociation rate from group g . Similarly, $K_{h,g}$ and C_g^r are the group deexcitation and recombination rate coefficients, respectively. The numerical index m on these rate coefficients corresponds to the moment for which they are being defined. Equation (15) shows the final form of the macroscopic equations that are solved in the multigroup maximum entropy quadratic model:

$$\begin{aligned} \frac{dn_g}{dt} &= \sum_{h \in \mathbf{N}} [-{}^0K_{g,h}n_gn_N + {}^0K_{h,g}n_hn_N] - {}^0C_g^d n_g n_N + {}^0C_g^r n_N^2 n_N, \\ \frac{de_g}{dt} &= \sum_{h \in \mathbf{N}} [-{}^1K_{g,h}e_gn_N + {}^1K_{h,g}e_hn_N] - {}^1C_g^d e_g n_N + {}^1C_g^r n_N^2 n_N, \\ \frac{df_g}{dt} &= \sum_{h \in \mathbf{N}} [-{}^2K_{g,h}f_gn_N + {}^2K_{h,g}f_hn_N] - {}^2C_g^d e_g n_N + {}^2C_g^r n_N^2 n_N. \end{aligned} \quad (15)$$

The grouped rate coefficients are expectation values of the function, $\langle \sum_{j \in I_h} k_{i,j} \varepsilon_i^m | i \in I_g \rangle$, normalized by the moment values written as $n_{\text{tot}} \langle X_g^m \rangle$, where $n_{\text{tot}} = \sum_{g \in \mathbf{N}} n_g$. The macroscopic group rate coefficients for the m th moment are given by Eqs. (16)–(19). Equation (16) gives the forward rates of a reaction, which lead to the depletion of the group moment, whereas Eq. (17) gives the reaction rates for the reverse processes populating the particular group. Note that, for $m = 0$, the group rate coefficient matrix is symmetric.

However, for higher moments the group rate coefficients need to be computed for both the forward and the reverse processes. mQ_g in these expressions denotes the m th moment group partition function for group g and is a normalization parameter which is expressed as a weighted sum of probabilities of finding a molecule in the energy levels belonging to a particular group. Equation (11) gives the form of the partition function.

It should be noted that the superscript m on ε_i is the m th power of the energy value. The recombination rates are simply a summation of the individual microscopic recombination rate coefficients of the states belonging to a particular group since these rates do not depend on the internal energy-state population distribution of the molecules. It is worth mentioning here that the principle of detailed balance for the grouped rates holds only when the quadratic coefficient goes to 0 and the internal temperatures corresponding to the β parameters for all the groups are the same and equal to the translational temperature. This condition is achieved only when the system is at equilibrium and is an important validation of the model since at equilibrium the forward and reverse processes should balance each other out. A thorough derivation of detailed balance between grouped rates is given by Macdonald in [49].

Group quantities are obtained by numerically integrating Eqs. (15) in time. We used the backward differentiation scheme of the CVODE package from SUNDIALS [48] for this purpose. At every time step, the macroscopic rate coefficients for each group are calculated as follows:

$$\begin{aligned} {}^mK_{g,h} &= \sum_{i \in I_g} \sum_{j \in I_h} \frac{k_{i,j} \varepsilon_i^m n_i}{n_{\text{tot}} \langle X_g^m \rangle} \\ &= \frac{1}{{}^mQ_g} \sum_{i \in I_g} \sum_{j \in I_h} k_{i,j} \varepsilon_i^m g_i \exp[-\beta_g \varepsilon_i - \gamma_g \varepsilon_i^2], \end{aligned} \quad (16)$$

$$\begin{aligned} {}^mK_{h,g} &= \sum_{i \in I_g} \sum_{j \in I_h} \frac{k_{j,i} \varepsilon_i^m n_j}{n_{\text{tot}} \langle X_h^m \rangle} \\ &= \frac{1}{{}^mQ_h} \sum_{i \in I_g} \sum_{j \in I_h} k_{j,i} \varepsilon_i^m g_j \exp[-\beta_h \varepsilon_i - \gamma_h \varepsilon_i^2], \end{aligned} \quad (17)$$

$$\begin{aligned} {}^mC_g^d &= \sum_{i \in I_g} \frac{k_i^d \varepsilon_i^m n_i}{n_{\text{tot}} \langle X_g^m \rangle} \\ &= \frac{1}{{}^mQ_g} \sum_{i \in I_g} k_i^d \varepsilon_i^m g_i \exp[-\beta_g \varepsilon_i - \gamma_g \varepsilon_i^2], \end{aligned} \quad (18)$$

$${}^mC_g^r = \sum_{i \in I_g} k_i^r \varepsilon_i^m. \quad (19)$$

This is required since the macroscopic group rate coefficients depend on the model parameters, and they change with time. To circumvent the actual summation, thermodynamic tables can be computed for the rates over a range of the linear and quadratic parameters, which can then be used to obtain the group rate coefficients by interpolation.

IV. VALIDATION AND RESULTS

The multigroup maximum entropy quadratic model is validated by comparison of the full state-to-state model with the solutions of the system of macroscopic governing equations, (15). The macroscopic governing equations represent a set of stiff, highly nonlinear ordinary differential equations which are difficult to solve. To integrate these equations in time, backward differentiation formulas from CVODE of the package SUNDIALS [48] were implemented. Determination of the group moment values, Eq. (15), with a good accuracy is essential in the calculation of the quadratic model parameters, α_g , β_g , and γ_g , which are functions of the group moments. However, these functions represent a system of coupled highly nonlinear equations and cannot be inverted to calculate the quadratic parameters directly. Therefore, it is necessary to use an iterative root-finding algorithm. Both CVODE and KINSOL use a LAPACK-based direct solver run in parallel using OpenMP.

The thermally and chemically reacting system in a nonequilibrium state is studied by carrying out isothermal simulations with no spatial variations. The translation temperature of the mixture is initialized to 2000 K, and the mixture is assumed to consist of 95% N₂ and 5% N. It is necessary to include some initial atoms to establish thermal excitation and chemical reactions since molecule-molecule collisions are not considered. The translation temperature of the reactor is then

increased to a higher temperature. Two cases are studied, one at 10 000 K and the other at 20 000 K. Translation modes of the N_2 -N system equilibrate to the translational temperature instantly. The strong thermal and chemical nonequilibrium state within the rovibrational levels of the N_2 molecule arising due to collisions is studied using the proposed model.

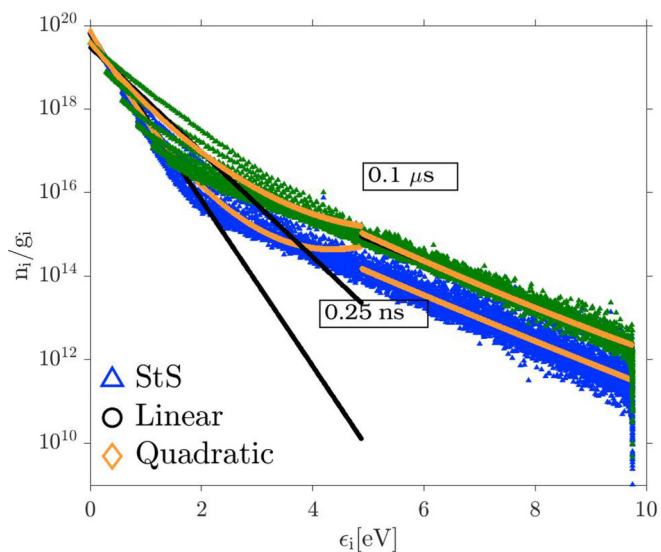
A. Comparison of the state population distribution

A comparison of the state population distribution is done for the quadratic model at various simulation times for two translational temperature cases, 10 000 and 20 000 K. To assess the quality of the reconstruction function, the results are plotted against the full StS solution. Simulations with two and three groups for the energy spectrum of the molecule are studied. Energy-based grouping [32] is employed for both linear and quadratic groups.

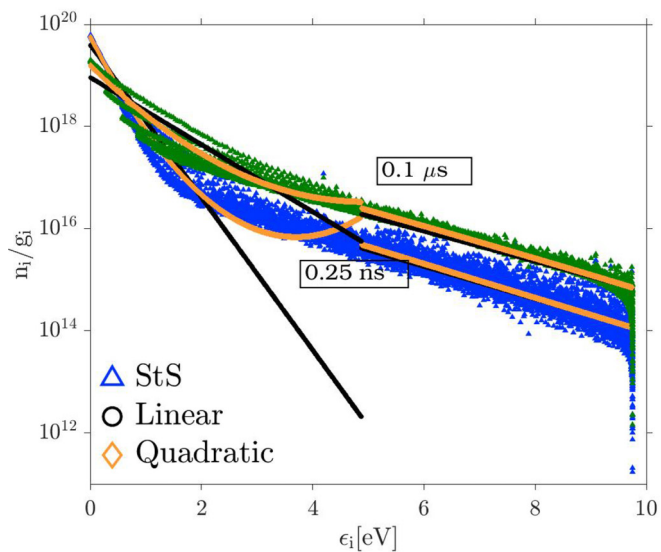
The distribution function temporally evolves from a Boltzmann distribution at 2000 K through transient non-Boltzmann distributions to a Boltzmann distribution at 10 000 or 20 000 K. The slope of the initial distribution is higher than the final distribution since the slope of the plot is inversely proportional to the temperature of the system: the higher the temperature, the lower the slope. During the initial phase, the higher levels start to approach the Boltzmann distribution at the final translation temperature, while the lower levels are at strong nonequilibrium. The purpose of the proposed model is to accurately represent this state of strong nonequilibrium.

Figure 3 shows the comparison of the population distribution for two groups at 10 000 and 20 000 K at two instants in time, $t = 0.2$ ns and $t = 0.1$ μ s. Looking at the population distribution for the two translation temperatures, we observe that the population of the lower states is of the same order of magnitude. This is expected since the lower states are initially in a frozen state at the starting translational temperature of 2000 K. It is shown that the first group of the linear model deviates significantly from the true distribution. In contrast, the first group in the quadratic model provides a better representation of the StS population distribution in both temperature cases. The ability of the quadratic model to account for the “curvature” in the distribution function helps to obtain a better description of the distribution function.

Figure 4 shows a comparison of the three models with three groups. Reconstruction using three quadratic groups shows a promising representation of the nonequilibrium behavior of the system at all times. As we march forward in time, it can be seen that the non-Boltzmann distributions are more accurately reconstructed using the quadratic model at the two instants in time. The moment values and, hence, the slope as well as the curvature values in the quadratic formulation change continuously such that the probability mass function for the energy states is reconstructed accurately as shown in Fig. 4. There are several advantages and obvious improvements in the results when using three groups instead of two. The most striking improvement is the representation of the distribution in the lower-energy states of the molecule. The dynamics of the nonequilibrium distribution in a chemical system with dissociation in general is such that the energy space of the molecule is naturally divided into three regions [12,24,50]. The first is comprised of the lower-energy states, which slowly



(a) $T = 10,000$ K



(b) $T = 20,000$ K

FIG. 3. Comparison of the state population distributions obtained using the state-to-state (triangles; blue at 0.25 ns and green at 0.1 μ s) and two-group maximum entropy linear (black circles) and quadratic (yellow diamonds) models. (a) $T = 10\,000$ K; (b) $T = 20\,000$ K.

relax to the final translation temperature, followed by the mid sloping region and, finally, the tail, where dissociation facilitates quick equilibration to the translational temperature. This makes three groups a naturally good choice for the division of the energy space of the molecule and leads to a better representation compared to the two-group maximum entropy quadratic model.

An observation worthy of mention is the reaction dynamics near the dissociation limit of the N_2 molecule, which is equal to 9.753 eV. Molecules which have energies very close to the dissociation limit dissociate quickly due to high dissociation rates, as shown in Fig. 5, which is a plot of the state-specific

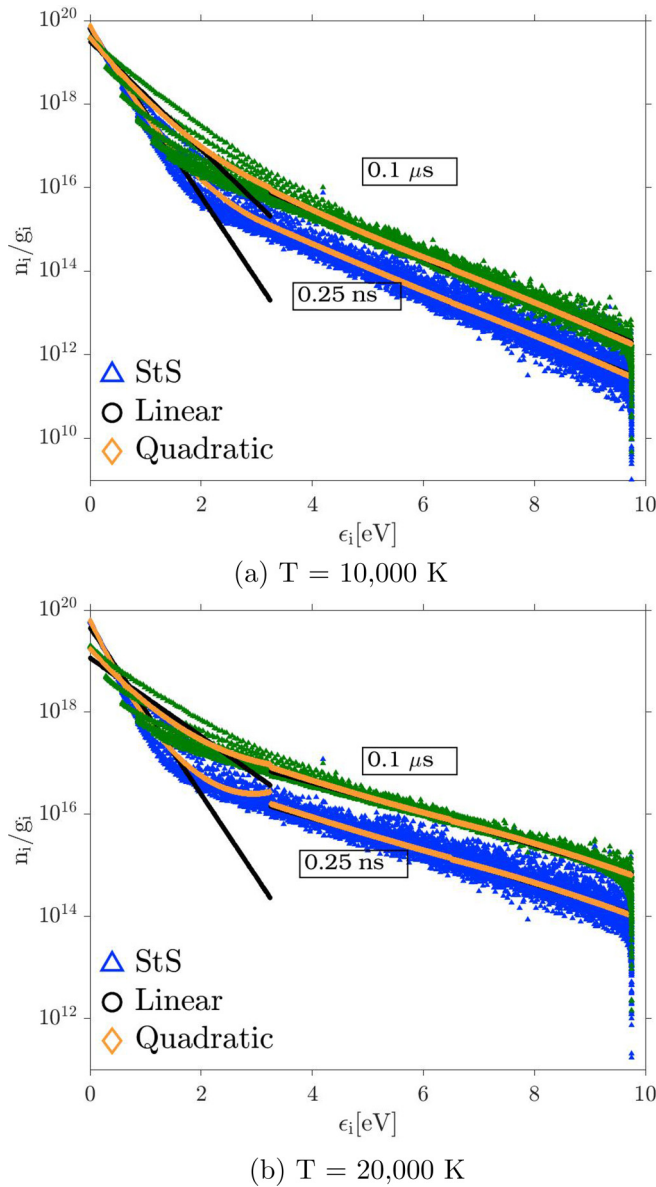


FIG. 4. Comparison of the state population distributions obtained using the state-to-state (triangles; blue at 0.25 ns and green at 0.1 μ s) and three-group maximum entropy linear (black circles) and quadratic (yellow diamonds) models. (a) $T = 10\,000$ K; (b) $T = 20\,000$ K.

dissociation rates plotted against the energy of the rovibrational levels. This causes the population to plummet at the dissociation limit as observed in the population distribution as the almost-vertical line.

Another interesting feature is observed in the full state population distribution at around 0.1 μ s. In the lower-energy states, distinct strands separate out [12]. As we move higher in the energy space, the strands coalesce into a cloud of particles. It is noted that the energy states connected by these strands have the same vibrational quantum number. Moreover, each vibrational strand is further divided into two different strands corresponding to the odd and even rotational quantum numbers belonging to that vibrational quantum number. This implies that the lower rotational states belonging to the same

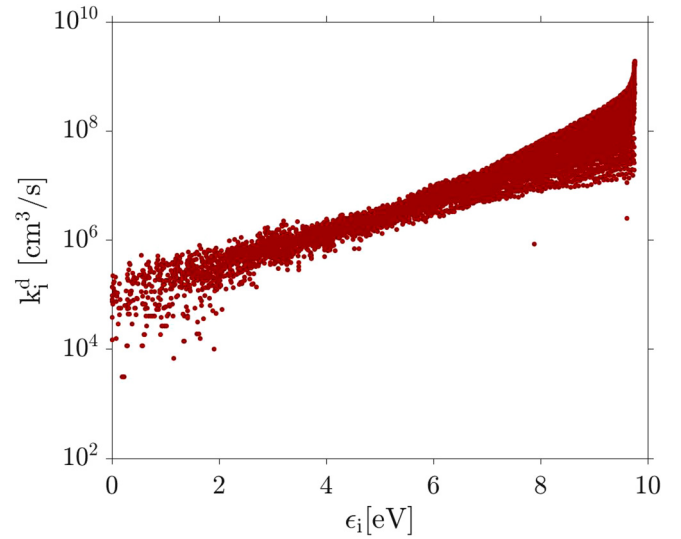


FIG. 5. State-specific dissociation rate constants for rovibrational states of N_2 .

vibration energy state tend to equilibrate more rapidly, giving rise to these strands. The quadratic model using two or three groups is able to provide an average representation of the curvature of these strands using equal energy spacing groups. However, it is not able to mimic the strands individually because, in the grouping strategy employed in this study, the kinetics of the chemical system is not considered as a grouping parameter. Recently, effort has been under way to understand the effect of kinetics on the grouping strategy as well as PMF reconstruction, e.g., by Sahai *et al.* [51] and Venturi *et al.* [50].

At all times, the quadratic model outperforms the linear model in the reconstruction of the full population distribution function. This can be attributed to the ability of the quadratic model to estimate the population distribution of the first group, which is highly underpredicted by the linear model. In the figures, it can also be seen that the quadratic model is able to reconstruct the population distributions for different profiles, one corresponding to a final translational temperature of 10 000 K and the other to a translational temperature of 20 000 K.

To quantitatively prove the usefulness and accuracy of the quadratic model, we look at the moment generating function of the probability mass function. It is a well-known fact in probability theory that in order to accurately estimate a distribution function it is necessary to be able to reproduce the moment generating function (if it exists) accurately. The moment generating function in general has the following form:

$$f(z) = \sum_{m=0}^{\infty} \frac{1}{m!} z^m E[X^m], \quad z \in \mathbb{R}. \quad (20)$$

Here, X is the discrete random variable which is analogous to the energy as described in Sec. III. Rewriting the moment generating function in terms of n_i and ϵ_i we get

$$f(z) = \sum_{m=0}^{\infty} \frac{1}{m!} \frac{z^m}{n_{\text{tot}}} \left(\sum_i n_i \epsilon_i^m \right), \quad z \in \mathbb{R}. \quad (21)$$

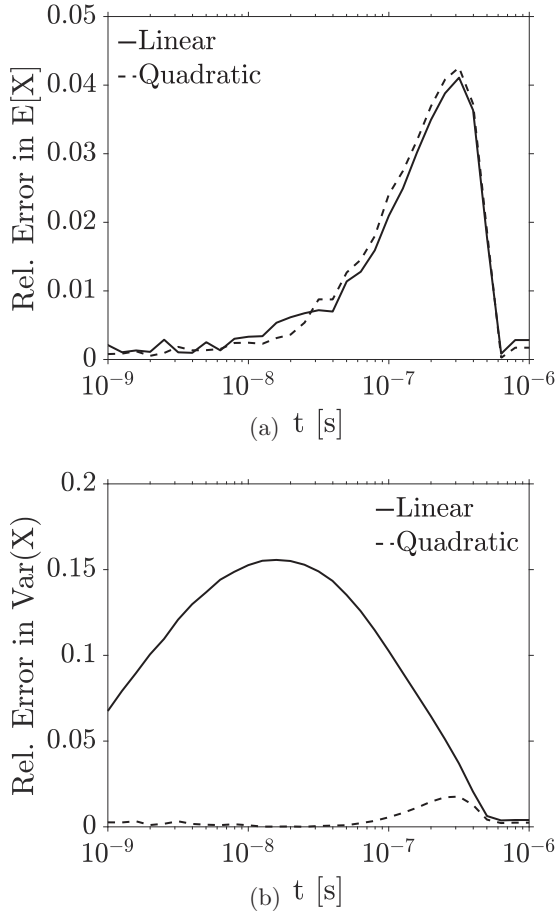


FIG. 6. Percentage error in mean and variance of the PMF estimated using three linear and quadratic groups. (a) Error in mean and (b) error in variance of the distribution function.

In the case of the quadratic model, the summation is truncated at $m = 2$, while in the linear model we have just the first-order linear terms. Therefore, the error in the quadratic function is inherently lower, $O(3)$, for each individual group, which quantitatively proves that the quadratic model works much better than the linear model. The mean and variance of the distribution function can be written as

$$E[X] = \sum_i \frac{n_i}{n_{\text{tot}}} \varepsilon_i,$$

$$\text{Var}(X) = \sum_i \frac{n_i}{n_{\text{tot}}} \varepsilon_i^2 - \left(\sum_i \frac{n_i}{n_{\text{tot}}} \varepsilon_i \right)^2. \quad (22)$$

Figure 6 shows a comparison of the error in the estimated mean and variance of the distribution function for the two models. The error is calculated as the deviation from the actual distribution obtained from the StS solution. As expected, the mean is estimated very accurately with both models, with errors of less than 4.5% throughout the relaxation process [Fig. 6(a)], since the first moment is solved for explicitly in both models. However, comparing the variance of the distribution, which gives a sense of the spread of the distribution, we see that the quadratic model greatly outperforms the linear model, with the error being less than 2%, while the linear

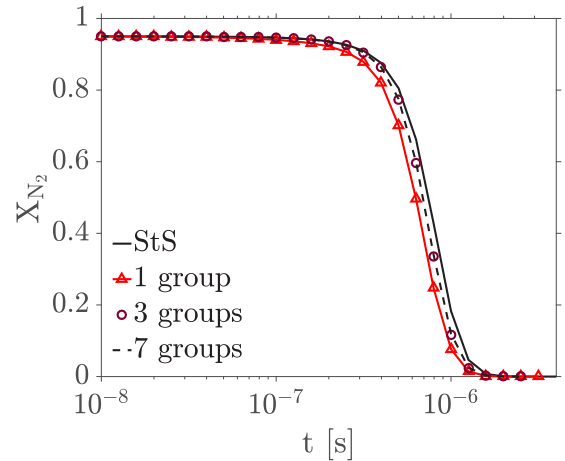


FIG. 7. Mole fraction profiles zoomed in during dissociation.

model incurs errors of up to 15% during the excitation phase when there is a large spread or variance in the distribution function. Closer to the dissociation phase, $t \approx 1 \mu\text{s}$, the population distribution is predominantly a straight line, and hence the error in $\text{Var}(X)$ of both models decreases significantly.

B. Comparison of the macroscopic quantities

This subsection presents a comparison of the time evolution of macroscopic quantities obtained with the quadratic model and the StS model for a heat-bath temperature of $T = 20\,000 \text{ K}$. In order to assess the sensitivity of the solution to the number of groups used in the reduced-order model, the simulations were run for one, two, three, five, and seven groups.

In Fig. 7, the predicted time evolution of the molecular nitrogen concentration is presented. Under these conditions, the bulk of the dissociation takes place only after a long incubation period, during which the kinetic energy is transferred to the internal energy modes. As a result, significant dissociation occurs only after $t = 3 \times 10^{-7} \text{ s}$. As the system evolves towards its final equilibrium state, the averaged internal energy of the system increases (see Fig. 8), and the high-lying excited states become significantly populated, thus increasing the effective macroscopic dissociation rate. The dissociation is completed and the system reaches chemical and thermal equilibrium by $3 \mu\text{s}$. Given the elevated temperatures, a significant portion of the dissociation process does not occur under quasi-steady-state (QSS) conditions [12]. The modeling of dissociation under non-QSS conditions is extremely challenging due to rapid changes in the internal distribution function that take place throughout the relaxation and the impossibility of defining a single macroscopic phenomenological rate coefficient able to describe the entire dissociation process [52]. This constitutes one of the main shortcomings of the state-of-the-art models built on the QSS assumption.

Comparison of the composition profiles reveals that the reduced-order model is able to describe the entire relaxation with a single group. The results obtained using a single group relax slightly faster compared to the StS prediction. This behavior can be attributed to inaccuracy in the description

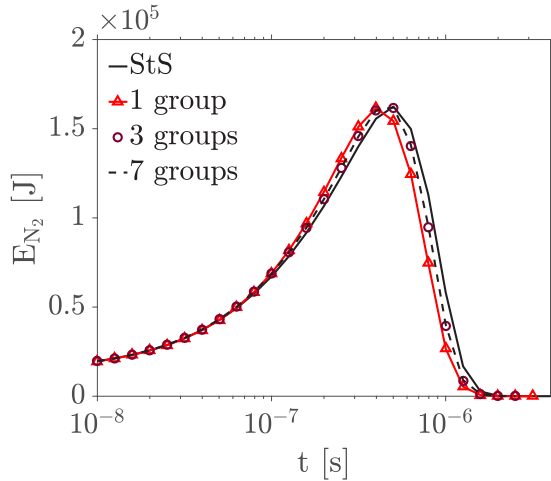


FIG. 8. Total internal energy.

of the high-lying levels in the distribution function. With the curvature parameter, the one-group reconstruction function is simply a parabolic profile in the internal energy space (Fig. 9). This leads to an overprediction of the population of the high-energy states which have high dissociation rates, as shown in Fig. 5, and results in a faster averaged dissociation rate; this comes directly from Eq. (18). As the number of groups is increased, the concentration profiles approach the StS solution. Figure 7 shows that the mole fraction values converge for groups 3 and 7. The excellent agreement obtained with the quadratic reconstruction model demonstrates the flexibility and generality of the method and, more importantly, its ability to describe both QSS and non-QSS regimes.

The analysis of the internal energy profiles, shown in Fig. 8, demonstrates the ability of the reduced model to predict the total internal energy of N_2 accurately. The internal energy of the N_2 molecules is initially almost a constant since there are very few excitation and dissociation events occurring at

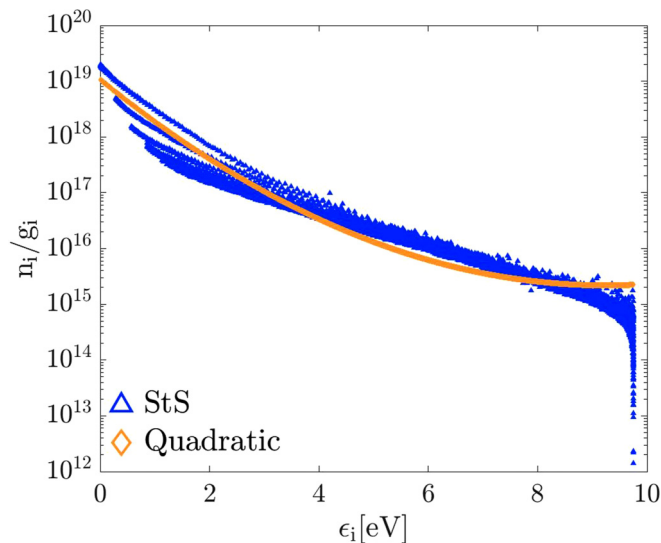


FIG. 9. State population distribution obtained from a one-group maximum entropy quadratic model compared with the actual distribution from the state-to-state model.

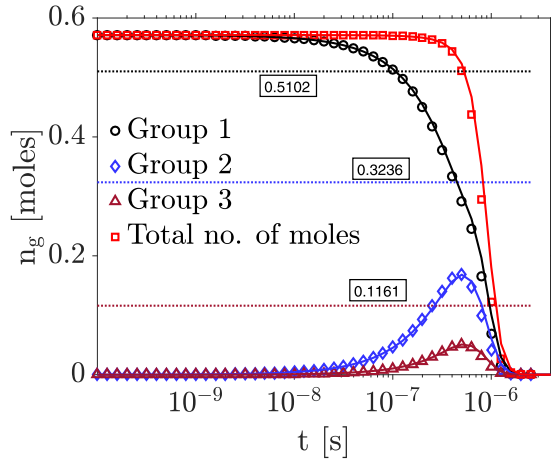
2000 K. As the system evolves, the internal energy of the nitrogen molecules increases, until the onset of dissociation, which depletes the number of molecules, thus reducing the internal energy of the molecular species in the gas. As discussed for Figs. 3 and 4, some deviation from the full StS simulation exists due to the type of grouping strategy (uniform energy grouping) employed in this paper. It is worth mentioning here that during this time evolution simulation, the total energy of the system is conserved, but not the group energy. However, the time scales for the group internal reactions are assumed to be much smaller than the time scales of intergroup processes and reactive processes, therefore, when looking at the evolution of the moments, it is a safe assumption that the properties within the group equilibrate with each other instantly. This leads to another approximate collision invariant, which is the group internal energy [49]. Since intergroup processes are still taking place at slower time scales, as seen in the evolution of group internal energies, this is what drives the system to the overall equilibrium state as time evolves.

C. Comparison of group properties

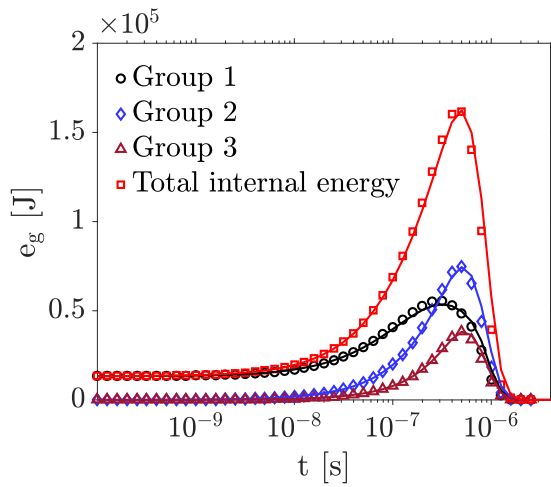
For the sake of brevity, the comparison of the group properties is shown only for the three-group quadratic model against the StS solution. Such a comparison has been done for different numbers of groups, and all cases yield similar results. The group properties from the StS simulation are calculated by taking moments of the actual distribution in the postprocessing step since the output from the StS simulation directly gives the population in each energy state.

Figure 10(a) shows a comparison of the number of moles in each group. The solid lines represent the StS results and the markers represent the quadratic model. The prediction of the quadratic model are in excellent agreement with the StS results. In the early stages of the relaxation only the first group is significantly populated, and throughout the relaxation its density decreases monotonically as the higher groups are excited. This trend is in contrast to the evolution of the number of moles in higher groups. The initial number of moles in the higher groups is very low because at a temperature as low as 2000 K most of the molecules are in the ground state or occupy the lower-energy states. As time evolves, the excitation reactions from the lower groups cause the mole fractions of the higher groups to increase and eventually reach a maximum. In the early stages of the relaxation, excitation processes tend to drive the populations of the groups towards their corresponding equilibrium values at the final translational temperature. In the figure, these values are indicated by dotted lines. Given the elevated temperatures, the thermal relaxation is not completed at the onset of dissociation, indicating that thermal and chemical relaxation occur concurrently. The onset of dissociation causes the number of moles to decrease, thus affecting the group populations. It is important to note that the lower-temperature case did not exhibit this behavior, and the thermal and chemical relaxation were found to be decoupled.

Figure 10(b) shows a comparison of the internal energy of each group. All groups have similar trends for the evolution of the group internal energy. Group 1 shows a higher internal energy at the start of the simulation because the lower-energy states are the most highly populated. The second group



(a) Group no. of moles



(b) Group Internal Energy

FIG. 10. Time evolution of the number of moles in each group and the group energy. Symbols represent the quadratic model and solid lines represent the full state-to-state model. (a) Group number of moles; (b) group internal energy.

becomes populated significantly due to pumping of molecules from the first group through excitation. It is important to note that the faster relaxation of the second group is mainly due to the presence of exchange reaction processes that favor the energy transfer between the levels characterized by energies between 3 and 8 eV. Furthermore, the states belonging to the second group are characterized by higher energies, thus contributing more to the total energy of the group. The latter group is in general not very highly populated; furthermore, its population is significantly depleted due to the very fast dissociation processes. This explains its low energy content.

Another important physical macroscopic quantity studied is the internal temperature of each group. The temperature for each group is computed using the energy-state population distribution. To calculate the temperature, the following one-dimensional nonlinear equation is solved:

$$\frac{e_g}{n_g} = \frac{1}{Q_g} \sum_{i \in I_g} g_i \varepsilon_i e^{-\varepsilon_i/k_B T_g}. \quad (23)$$

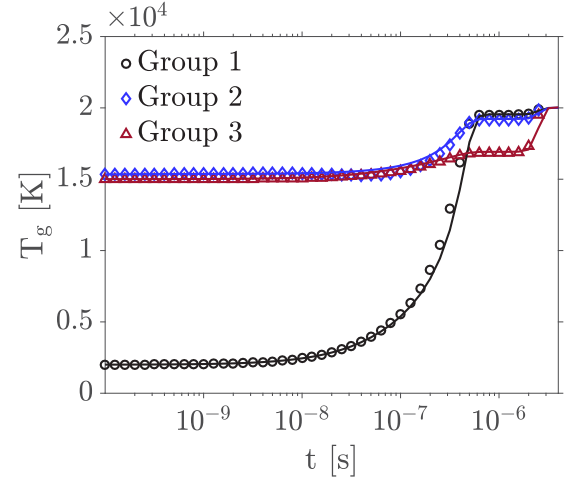


FIG. 11. Time evolution of the group internal temperature. Symbols represent the quadratic model and solid lines represent the full state-to-state model.

It is important to clarify that a linear reconstruction function is used to compute the moments of the distribution function where the linear term coefficient is inversely proportional to the internal temperature of the group. The simulation starts at a temperature of 2000 K and progresses to equilibration at 20 000 K. In Fig. 11, a comparison of the temperatures obtained from the StS and quadratic solutions at different times shows good agreement. All groups attain a final temperature of 20 000 K, the temperature of the reactor.

Groups 2 and 3 quickly first reach quasi-steady state, at about 15 000 K. The onset of dissociation alters the temperature of the three groups: groups 1 and 2 are at QSS at the same temperature, while the third group exhibits a significantly lower temperature due to the effect of dissociation. All three groups equilibrate at the final temperature at the end of the relaxation.

D. Comparison of group parameters

In this section, we present a discussion of the model parameters β and γ . These model parameters are related to the slope and curvature of the population distribution. The values of β and γ are of the order of the energy and the energy squared, respectively. Dealing with model parameters of such different orders of magnitude poses computational challenges. Hence, to work with more reasonable values of β and γ , the energy and model parameters are normalized. The normalization constant used is the value of the dissociation limit of the nitrogen molecule, 9.753 eV ($\equiv \hat{\varepsilon}$). These new normalized parameters are distinguished by hats, $\hat{\beta}$ and $\hat{\gamma}$, and are related to the actual values by the following equations:

$$\hat{\beta} = \beta \hat{\varepsilon}, \quad (24)$$

$$\hat{\gamma} = \gamma \hat{\varepsilon}^2. \quad (25)$$

Figure 12 shows the evolution of the quadratic parameters for three groups. The results for $\hat{\beta}$ are similar to those obtained for the internal temperatures, therefore similar considerations apply to this parameter. The value of the first group is

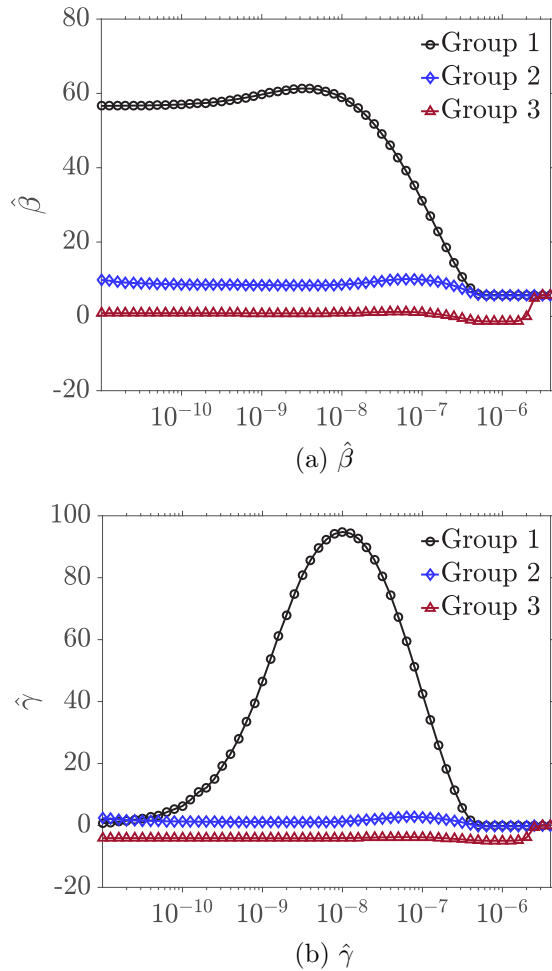


FIG. 12. Time evolution of quadratic parameters using three groups. (a) $\hat{\beta}$; (b) $\hat{\gamma}$.

substantially frozen in the initial stages of the relaxation, while groups 2 and 3 quickly reach lower values of $\hat{\beta}$. During dissociation, $\hat{\beta}$ of group 3 decreases to a negative value. This negative value for group 3 should not be confused with a population inversion. This value of $\hat{\beta}$ is just a parameter in the quadratic model which is combined with the quadratic terms. These two terms together define the population distribution of this group. A negative value is also observed for $\hat{\gamma}$ due to the inverted parabolic shape of the population distribution near the dissociation limit.

Analysis of the time evolution of the $\hat{\gamma}$ parameter reveals that significant curvature is necessary for the first group, while the other two groups could be treated using a linear model. As reported in Sec. IV A, the population distribution follows a non-Boltzmann distribution, where the lower-lying states are frozen while the high-lying states are significantly excited.

Figure 12 shows that, as the system approaches equilibrium, the $\hat{\beta}$ and $\hat{\gamma}$ values of all groups start to converge. When the system reaches equilibrium the distribution reaches the Boltzmann distribution. The value of β_g for each group can be shown to be related to the Boltzmann constant (k_B) and the

final equilibrium temperature of the system by

$$\beta_g = \frac{1}{k_B T}, \quad (26)$$

and we get

$$\frac{n_i}{n_{\text{tot}}} = \frac{g_i \exp\left[-\frac{\varepsilon_i}{k_B T}\right]}{\sum_{j \in I_n} g_j \exp\left[-\frac{\varepsilon_j}{k_B T}\right]}. \quad (27)$$

On the other hand, the value of $\hat{\gamma}$ and, by extension, the curvature of the distribution functions tend to 0 as the system approaches equilibrium. This result is consistent with the derivation of β_g and physically means that the distribution approaches the Boltzmann distribution at the final translational temperature. This constitutes an important validation of the proposed method, since, at equilibrium, the molecules attain a Boltzmann distribution and hence all higher-order terms in the description of the population distribution must become 0, i.e., $\hat{\gamma}$ values for all groups approach 0.

V. CONCLUSION

In summary, this paper presents an advanced technique to model nonequilibrium flows for thermal nonequilibrium and state-specific chemical kinetics based on the method of moments combined with an energy-based grouping strategy. This model comprises a quadratic reconstruction operator to represent the logarithm of the population distribution function of the molecules in energy space. The kinetic and thermodynamic data are obtained from *ab initio* calculations performed at NASA Ames Research Center [1–11]. In the computation of group properties, no *ad hoc* assumptions are made, and hence this model retains most of the physics of the system. From the results we see that this simple model is capable of accurately representing the non-Boltzmann distributions occurring in strongly nonequilibrium regimes. The key contribution of this model over previous nonequilibrium models [32–34] is the introduction of the quadratic parameter in the PMF definition. This reduces the number of groups required to estimate the non-Boltzmann distribution and makes the integration into CFD applications [53] more feasible.

Although the model is used to characterize nonequilibrium in the $\text{N}_2(^1\Sigma_g^+)$ - $\text{N}(^4S_u)$ system in this paper, the proposed approach is general and the framework presented in the paper can be applied to any physical system for arbitrary physical conditions. Particular attention is, however, required when dealing with interaction between polyatomic molecules. First steps in this direction have been published recently by Macdonald *et al.* [45,46]. In that work, the authors have proposed the MGME-QCT method, in which the grouped kinetic properties can be calculated directly from scattering calculations, bypassing the need to compute state-to-state rates. Future work shall address the extension of the quadratic model for its application to MGME-QCT.

ACKNOWLEDGMENTS

The work by M.P.S. and M.P. was supported by the Air Force Office of Scientific Research Young Investigators Research Program FA9550-15-1-0132.

- [1] D. W. Schwenke, *Dissociation Cross Sections and Rates for Nitrogen*, Tech. Rep., DTIC Document (Defense Technical Information Center, Fort Belvoir, VA, 2009).
- [2] G. M. Chaban, R. L. Jaffe, D. W. Schwenke, and W. M. Huo, in *46th AIAA Aerospace Sciences Meeting and Exhibit* (AIAA, 2008), pp. 2008–1209.
- [3] R. Jaffe, D. Schwenke, G. Chaban, and W. Huo, in *46th AIAA Aerospace Sciences Meeting and Exhibit* (American Institute of Aeronautics and Astronautics, Reston, VA, 2008), p. 1208.
- [4] R. L. Jaffe, D. W. Schwenke, and G. M. Chaban, in *47th AIAA Aerospace Sciences Meeting including The New Horizons Forum and Aerospace Exposition* (AIAA, 2009), pp. 2009–1569.
- [5] R. Jaffe, D. W. Schwenke, and G. M. Chaban, *10th AIAA/ASME Joint Thermophysics and Heat Transfer Conference* (AIAA, 2010), pp. 2010–4517.
- [6] J. Z. Zhang and W. H. Miller, *Chem. Phys. Lett.* **153**, 465 (1988).
- [7] D. W. Schwenke, *J. Chem. Phys.* **89**, 2076 (1988).
- [8] F. Esposito, M. Capitelli, and C. Gorse, *Chem. Phys.* **257**, 193 (2000).
- [9] D. Wang, J. R. Stallcop, W. M. Huo, C. E. Dateo, D. W. Schwenke, H. Partridge, and D. Kwak, *J. Chem. Phys.* **118**, 2186 (2003).
- [10] F. Esposito, I. Armenise, and M. Capitelli, *Chem. Phys.* **331**, 1 (2006).
- [11] F. Esposito and M. Capitelli, *Chem. Phys. Lett.* **302**, 49 (1999).
- [12] M. Panesi, R. L. Jaffe, D. W. Schwenke, and T. E. Magin, *J. Chem. Phys.* **138**, 044312 (2013).
- [13] J.-L. Cambier and S. Moreau, in *AIAA, 24th Plasmadynamics and Lasers Conference, Vol. 1* (American Institute of Aeronautics and Astronautics, Reston, VA, 1993).
- [14] M. Capitelli, I. Armenise, D. Bruno, M. Cacciatore, R. Celiberto, G. Colonna, O. De Pascale, P. Diomede, F. Esposito, C. Gorse *et al.*, *Plasma Sources Sci. Technol.* **16**, S30 (2007).
- [15] E. Josyula, W. F. Bailey, and S. M. Ruffin, *Phys. Fluids (1994–present)* **15**, 3223 (2003).
- [16] M. Panesi and A. Lani, *Phys. Fluids* **25**, 057101 (2013).
- [17] M. Kapper and J.-L. Cambier, *J. Appl. Phys.* **109**, 113308 (2011).
- [18] M. Kapper and J.-L. Cambier, *J. Appl. Phys.* **109**, 113309 (2011).
- [19] A. Munafò, M. G. Kapper, J.-L. Cambier, and T. E. Magin, in *50th AIAA Aerospace Sciences Meeting including the New Horizons Forum and Aerospace Exposition* (AIAA, 2012), pp. 2012–647.
- [20] C. Park, *Nonequilibrium Hypersonic Aerothermodynamics* (Wiley, New York, 1990).
- [21] C. Park, *J. Thermophys. Heat Transfer* **3**, 233 (1989).
- [22] C. Park, *J. Thermophys. Heat Transfer* **7**, 385 (1993).
- [23] C. Park, R. L. Jaffe, and H. Partridge, *J. Thermophys. Heat Transfer* **15**, 76 (2001).
- [24] E. V. Kustova and E. A. Nagnibeda, *Chem. Phys.* **208**, 313 (1996).
- [25] B. F. Gordiets, A. I. Osipov, and L. A. Shelepin, *Kinetic Processes in Gases and Molecular Lasers* (Moscow Izdatel Nauka, 1980).
- [26] C. E. Treanor, J. W. Rich, and R. G. Rehm, *J. Chem. Phys.* **48**, 1798 (1968).
- [27] E. V. Kustova, E. A. Nagnibeda, T. Y. Alexandrova, and A. Chikhaoui, *Chem. Phys.* **276**, 139 (2002).
- [28] A. Chikhaoui, E. A. Nagnibeda, E. V. Kustova, and T. Y. Alexandrova, *Chem. Phys.* **263**, 111 (2001).
- [29] M. Panesi, T. E. Magin, A. Bourdon, A. Bultel, and O. Chazot, *J. Thermophys. Heat Transfer* **25**, 361 (2011).
- [30] Y. Liu, M. Vinokur, M. Panesi, and T. Magin, in *10th AIAA/ASME Joint Thermophysics and Heat Transfer Conference* (AIAA, 2010), pp. 2010–4332.
- [31] Y. Liu, M. Panesi, M. Vinokur, and P. Clarke, in *44th AIAA Thermophysics Conference* (AIAA, 2013), pp. 2013–3146.
- [32] Y. Liu, M. Panesi, A. Sahai, and M. Vinokur, *J. Chem. Phys.* **142**, 134109 (2015).
- [33] A. Guy, A. Bourdon, and M.-Y. Perrin, *Chem. Phys.* **420**, 15 (2013).
- [34] H. P. Le, A. P. Karagozian, and J.-L. Cambier, *Phys. Plasmas* **20**, 123304 (2013).
- [35] T. E. Magin, M. Panesi, A. Bourdon, R. L. Jaffe, and D. W. Schwenke, *Chem. Phys.* **398**, 90 (2012).
- [36] A. Munafò, M. Panesi, and T. E. Magin, *Phys. Rev. E* **89**, 023001 (2014).
- [37] A. Munafò and T. E. Magin, *Phys. Fluids* **26**, 097102 (2014).
- [38] A. Munafò, Y. Liu, and M. Panesi, *Phys. Fluids* **27**, 127101 (2015).
- [39] A. Munafò, N. N. Mansour, and M. Panesi, *Astrophys. J.* **838**, 126 (2017).
- [40] I. Procaccia and R. Levine, *J. Chem. Phys.* **63**, 4261 (1975).
- [41] R. D. Levine and R. D. Bernstein, *Molecular Reaction Dynamics and Chemical Reactivity* (Oxford University Press, New York, 1987).
- [42] P. L. Varghese and D. A. Gonzales, in *Molecular Physics and Hypersonic Flows*, edited by M. Capitelli (Springer, Dordrecht, Netherlands, 1996), pp. 105–114.
- [43] M. Kulakhmetov, M. Gallis, and A. Alexeenko, *J. Chem. Phys.* **144**, 174302 (2016).
- [44] M. Massot, F. Laurent, D. Kah, and S. D. Chaisemartin, *SIAM J. Appl. Math.* **70**, 3203 (2010).
- [45] R. L. Macdonald, R. L. Jaffe, D. W. Schwenke, and M. Panesi, *J. Chem. Phys.* **148**, 054309 (2018).
- [46] R. L. Macdonald, M. S. Grover, T. E. Schwartzentruber, and M. Panesi, *J. Chem. Phys.* **148**, 054310 (2018).
- [47] M. Sharma Priyadarshini, M.S. thesis, University of Illinois at Urbana-Champaign, 2017.
- [48] A. C. Hindmarsh, P. N. Brown, K. E. Grant, S. L. Lee, R. Serban, D. E. Shumaker, and C. S. Woodward, *ACM Trans. Math. Software (TOMS)* **31**, 363 (2005).
- [49] R. L. Macdonald, Ph.D. dissertation, University of Illinois at Urbana-Champaign, 2019.
- [50] S. Venturi, M. P. Sharma, and M. Panesi, in *AIAA Scitech 2019 Forum, San Diego, CA* (American Institute of Aeronautics and Astronautics, Reston, VA, 2019).
- [51] A. Sahai, B. Lopez, C. Johnston, and M. Panesi, *J. Chem. Phys.* **147**, 054107 (2017).
- [52] M. Panesi, A. Munafò, T. E. Magin, and R. L. Jaffe, *Phys. Rev. E* **90**, 013009 (2014).
- [53] M. P. Sharma, S. Venturi, A. Munafò, and M. Panesi, in *AIAA Scitech 2019 Forum, San Diego, CA* (American Institute of Aeronautics and Astronautics, Reston, VA, 2019).